Mechanisms of hardening due to copper precipitates in α-iron

David John Bacon, Yuri Osetsky

Mechanisms of hardening due to copper precipitates in α-iron

Journal:	*Philosophical Magazine & Philosophical Magazine Letters*
Manuscript ID:	TPHM-09-Jun-0236.R1
Journal Selection:	Philosophical Magazine
Date Submitted by the Author:	28-Jul-2009
Complete List of Authors:	Bacon, David; University of Liverpool, Engineering Osetsky, Yuri; Oak Ridge National Laboratory
Keywords:	atomistic simulation, dislocations, molecular dynamic simulations
Keywords (user supplied):	Fe-Cu alloy, copper precipitates, alpha-iron

For special issue of Philosophical Magazine to mark 25 years of F-S potentials

Mechanisms of hardening due to copper precipitates in α-iron

D.J. Bacon[1*] and Yu.N. Osetsky[2]

[1)] Department of Engineering, The University of Liverpool, Liverpool L69 3GH, UK

[2)] Oak Ridge National Laboratory, P. O. Box 2008, Oak Ridge, TN 37831-6158 USA

ABSTRACT

A comprehensive atomic-level simulation study has been made of interactions between a moving edge dislocation and copper precipitates that are initially coherent with the body-centred-cubic matrix of alpha-iron Precipitates with diameter, D, in the range from 0.7 to 6 nm have been considered over the temperature range from 0 to 600 K. For some combinations of temperature and D, the critical applied resolved shear stress, τ_c, at which the dislocation overcomes a row of precipitates with centre-to-centre spacing, L, is consistent with an elasticity treatment for strong obstacles, e.g. τ_c is proportional to L^{-1} and ln(D). This has a specific atomic-level origin, for the proportionality holds when the dislocation induces a partial transformation of the copper towards the more stable face-centred-cubic phase. The driving force for the transformation increases with decreasing temperature and increasing D, and so τ_c has a strong temperature-dependence for large D. The results of these simulations, which employ a set of interatomic potentials of Finnis-Sinclair type, are seen to correspond well with experiments carried out elsewhere.

Keywords: Fe-Cu alloy; copper precipitates; alpha-iron; dislocations; molecular dynamics.

* Corresponding author:
e-mail djbacon@liv.ac.uk
tel. 0151 794 4662

1. Introduction

In the 25 years since the seminal paper by Finnis and Sinclair (F-S) [1] that introduced the many-body interatomic potential formalism which bears their name, one of the most widely used potential set is that for the Fe-Cu system in [2]. There are several reasons for this. First and foremost, there was, and still is, strong interest in the properties of atomic-scale defects in α-iron and its alloys, driven by the need to understand and predict the behaviour of ferritic materials in existing and next-generation nuclear power systems. Exposure to fast neutrons from the fission reaction generates radiation damage in the form of point defects and their clusters, and the evolution of this damage with time can give rise to changes in dimensions and mechanical properties. The nature and magnitude of the changes depend on the properties of the vacancy and interstitial defects and their interaction with other microstructure features such as dislocations. These properties and interactions are determined by atomic-level features and so require simulation at that scale. In the multiscale framework of material modelling, the results of this simulation can be used in higher-level treatments based on either Monte Carlo or continuum approximations.

Copper (Cu) in iron (Fe) is important because Cu-rich precipitates of small size (diameter D < few nm) form during neutron irradiation of ferritic pressure vessel steels that contain small amounts (a few tenths of a percent) of Cu. Cu precipitates that nucleate during thermal ageing of Fe-Cu alloys transform martensitically as they grow from the body-centred cubic (BCC) crystal structure coherent with the Fe matrix to a twinned 9R form of the face-centred cubic (FCC) structure. The size at which they transform from BCC to 9R falls in the range from about 4 to 10nm, depending on the heat treatment (e.g. [3]). In neutron-irradiated steels, however, Cu precipitates remain small and BCC in structure. Together with radiation damage formed by vacancies and self-interstitial atoms, they make a significant contribution to the radiation hardening associated with changes such as loss of ductility and increase of ductile-to-brittle transition temperature (e.g. [4-6]). Interaction between moving dislocations and precipitates is the cause of these effects and understanding of the atomic-scale mechanisms involved is therefore necessary for creation of predictive models of materials properties.

The Fe-Cu interatomic potential set in [2] has been widely used because the Fe-Fe potential had improvements for several crystal and defect properties over that in the original

F-S paper. Also, the form of the 1984 potential was different from that of the later F-S-type Cu-Cu potential of developed in [7], which was the basis of the Cu-Cu and Cu-Fe potentials in [2], and so lacked compatibility for a common computer code. (Readers are referred to original paper [2] for more information on the methodology and details of the parameters used in the potentials.) The Fe-Fe, Cu-Cu and Fe-Cu set of potentials has been widely used for simulation of phenomena such as displacement cascades, e.g. [8-12]; point defect clusters, e.g. [2,13-18]; defect diffusion in Fe-Cu alloys, e.g. [19-21]; properties of dislocation loops and stacking fault tetrahedra [22]; dislocation-void interaction, e.g. [23-26]; dislocation-dislocation loop interaction, e.g. [27,28]; dislocation- stacking fault tetrahedron interaction [29,30]; dislocation-Cu precipitate interaction in Fe, e.g. [31,32]; Cu precipitate properties and transformation, e.g. [33-36]. The references cited represent just a few of those in the published literature. Other potentials for the Fe-Cu system, such as [37], have not been employed so widely. Although the Fe-Fe potential in [38] has since provided a model that offers a better description of self-interstitial atoms and the screw dislocation core, an Fe-Cu set based on it has not been derived. Hence, the results of the present paper have been obtained by using the potentials for Fe-Cu from [2].

We have simulated the interaction between an *edge* dislocation gliding under stress and a row of spherical Cu precipitates with their equatorial plane coincident with the dislocation slip plane. The modelling method is described in section 2. The results for molecular static (MS) simulations which model systems at temperature, T, equal to 0 K are presented in section 3. This adds to the data for small precipitates given in [31]. Molecular dynamics (MD) simulations of dislocation-precipitate interaction at $T > 0$ K are presented in section 4. This adds to the data for small precipitates and lower temperature in [32]. Other issues, such as the effect of applied strain rate when $T > 0$ K, are discussed in section 5.

2. Model

The modelling method is described in detail in [39]. In summary, the BCC crystal was constructed with x, y, z axes parallel to [111], $[\bar{1}\,\bar{1}2]$, $[1\,\bar{1}0]$. We simulate an infinitely long, straight edge dislocation lying parallel to the y-axis with Burgers vector $\boldsymbol{b}$ = ½[111]. Periodic boundary conditions were applied along y in order to simulate a row of precipitates

with centre-to-centre spacing L, which equals the model size L_y. Values of L in the range 41.4 to 83.6nm were considered. In order to avoid restrictions on dislocation movement due to fixed boundary conditions, periodicity was also imposed along x, i.e. an array of edge dislocations with period equal to the model size L_x was simulated. Tests were made as in [39] to ensure that L_x was large enough to avoid model-size effects on dislocation behaviour. Values of L_x in the range 30 to 120nm were used for the smallest to largest precipitates. The model was bounded by rigid slabs of atoms in the z direction. The size, L_z, in this direction was 20nm for all cases, i.e. the models contained approximately two to eight million atoms. The Cu precipitates were coherent with the surrounding BCC matrix of Fe and as near spherical in shape as possible. Precipitates with diameter, D, in the range 0.9 to 6nm were modelled: they contained from 59 to 9698 Cu atoms.

Two qualitatively different techniques were used to simulate the dislocation overcoming these obstacles. For MS simulation (T = 0 K), resolved shear strain, $\varepsilon = \varepsilon_{xz}$, was applied in increments of 10^{-4} with relaxation to minimise of the model potential energy at each step. The corresponding resolved shear stress, $\tau = \sigma_{xz}$, was calculated from the total force exerted by the mobile atoms on the atoms in the rigid slabs at the z boundaries [39]. For the MD simulations (T > 0 K), applied shear strain rate, $\dot{\varepsilon}$, was imposed with values in the range 0.1×10^6 to 50×10^6 s^{-1}. The time-step was in the range 10 to 2 fs for T in the range 1 to 600 K, and τ was computed as above. Stress-strain plots were obtained in both the MS and MD studies and the critical shear stress, τ_c, for the dislocation to move through the array of obstacles was determined from the maximum value of τ. Identification and visualisation of the atomic structure of the obstacle and dislocation are important, and analysis of the location of the dislocation core was carried out at each strain increment in MS modelling and every 100 time-steps in MD. The method used is described in [39].

3. Simulation of strengthening at T = 0 K

As examples of the dependence of applied stress on strain at T = 0 K, Figure 1 shows τ versus ε plots for L = 41.4 nm and D in the range 1 to 5 nm. (The labels below each curve indicates D. For clarity, the graph for D = 6 nm is not included because the strain required for the dislocation to overcome the obstacle exceeds 2.6%.) The edge dislocation was

initially a few nm from the row of precipitates and the plots show that it starts to glide when τ rises to 24 MPa, which is the Peierls stress value for ½[111](1$\bar{1}$0) slip in this model of pure Fe. The dislocation is attracted into a precipitate when close to it, resulting in a reduction in potential energy, despite the fact that a step corresponding to ***b*** is created at the Fe-Cu interface. The energy change is associated with a lower core energy of the dislocation in BCC Cu. As a consequence, the plastic strain due to dislocation movement is larger than the imposed strain and τ is seen to become negative. The dislocation segment inside a precipitate resists further glide and so as ε continues to increase, the dislocation bows between the precipitates until it breaks away at τ_c.

It is found that the mechanism giving rise to the obstacle resistance of a precipitate changes as D increases. This is reflected in the shape of the stress-strain plot, as seen in Figure 1, and both τ_c and the line shape at this critical stress. The shapes for L = 62 nm and values of D up to 5 nm are shown by visualization of the dislocation core atoms and Cu atoms on the precipitate surface in Figure 2. The critical line shapes for voids over the same size range are included in the Figure for comparison. The label for each pair of lines indicates from top to bottom: τ_c for the void, D and τ_c for the precipitate. (The shape for the 6 nm precipitate could not be included in Figure 3 at the length scale used because the parallel screw arms at the precipitate surface extend to a length >100 nm before breakaway at τ_c = 292 MPa.) The critical angle, φ_c, subtended by the dislocation segments at the obstacle surface is shown for one of the precipitates. This angle provides an indication of the obstacle strength (see below) and is seen to change from a large value (~170°) for D = 0.9 nm to 0° for D = 5 nm, in contrast to a value of 0° for all but the smallest voids.

Values of τ_c for precipitates are plotted (triangle symbols) in Figure 3 against the harmonic mean $(D^{-1}+L^{-1})^{-1}$ on a log scale for all the combinations of D and L considered. The units of the ordinate and abscissa are Gb/L and b, respectively, where G is the elastic shear modulus. The reason for plotting the data in this way is that the following correlation between these quantities was found in the computer-based elasticity treatment with dislocation self-stress included of strengthening by impenetrable obstacles (Orowan strengthening) and voids [40,41]:

$$\tau_c = \frac{Gb}{2\pi L}\left[\ln\left(D^{-1}+L^{-1}\right)^{-1}+\Delta\right], \qquad (1)$$

where Δ equals 0.77 for the Orowan process and 1.52 for voids. G is chosen by setting $Gb^2/4\pi$ equal to the pre-logarithmic anisotropic energy factor of the screw dislocation of the ½<111>{110} system in Fe and is 64GPa [42]. Lines for the two value of Δ are drawn on Figure 3, which also contains data (circle symbols) for τ_c for an edge dislocation to overcome a periodic row of spherical voids in the same atomic MS model of Fe as used here [31,43,44]. The critical stress values for voids are seen fit equation (1) obtained from the continuum modelling well, except for the smallest size when D falls below 2 nm. For Cu precipitates, however, the correlation does not apply for D less than 4 nm and small precipitates are much weaker obstacles than voids of the same size. Only the largest precipitates of the range considered result in τ_c comparable with that for voids.

The explanation for the D- and L-dependence of τ_c for voids and impenetrable Orowan particles is that they are 'strong' obstacles to dislocation motion and so the dislocation segments at the obstacle surface are pulled into parallel, dipole alignment at τ_c by the combination of τ and self-interaction [40,41]. For every obstacle, the forward force, $\tau_c bL$, on the dislocation has to match the dipole tension, i.e. energy per unit length, which is proportional to ln(D) when $D<<L$ and ln(L) when $L<<D$, e.g. [45]. Thus, $\tau_c bL$ correlates with $Gb^2\ln(D^{-1} + L^{-1})^{-1}$ and the continuum approximation applies for voids of size down to 1-2 nm.

The significant differences between τ_c of precipitates and voids for D less than 4 nm arise because although the potential energy of the crystal is lowered when the dislocation enters a precipitate, the dislocation core energy is not zero in the Cu and the Cu-Fe interface has lower energy than the free-surface step on a void. Consequently, the dislocation is released from the precipitate rather easily and simply shears it without being pulled into screw orientation, as can be seen by the line shapes in Figure 2. For example, the critical included angle, φ_c, is 70° for the 3 nm precipitate compared with 0° for the void of the same size.

The screw dipole configuration is achieved at τ_c for D = 4 nm and the critical line shapes for the precipitate and void are almost indistinguishable for $D \geq 5$ nm. The τ_c values are correspondingly close. The mechanism that controls the process is different for the two obstacles, however. This effect arises from the dependence on D of the stability of the BCC

structure of Cu in a precipitate, as first noted in [31]. The BCC Cu in the larger precipitates undergoes a dislocation-induced, partial transformation to a more stable FCC-like structure. This is demonstrated in Figure 4(a) by the projection of atom positions in four $(1\bar{1}0)$ atomic planes near the equator of a 4 nm precipitate after dislocation breakaway at 0 K. The {110} planes have a two-fold stacking sequence in the BCC metals, as can be seen by the upright and inverted triangle symbols near the outside of the precipitate, but atoms represented by circles are in a different sequence. Atoms away from the Fe-Cu interface are seen to have adopted a three-fold sequence characteristic of the {111} planes in an FCC metal. Figure 4(b) shows the stacking arrangement after dislocation breakaway from a 6 nm precipitate. (The value of T was 10 K rather than 0 K, but the effect on the transformation of temperature at low values is slight.) There is a thin layer of BCC stacking due to coherency with the Fe matrix, but the volume of transformed material is much larger in the larger precipitate.

This dislocation-induced, permanent transformation of the precipitate structure, first found in MS simulation of a screw dislocation penetrating a precipitate [46], increases the obstacle strength, as shown by the shape of the dislocation in the $(1\bar{1}0)$ glide plane at $\tau = \tau_c$. These atomic-level mechanisms are not predicted by continuum treatments, such as the line-tension and modulus-difference approximations that form the basis of the Russell-Brown model of Cu precipitate strengthening of Fe [47].

4. Simulation of strengthening at $T > 0$ K

As the temperature increases from 0 K, τ_c decreases and the dislocation line bows out less in the critical condition. However, the variation with T of the form of the stress-strain curve, the critical line shape and τ_c depends on D, unlike the situation with voids. The dependence of τ_c on T for all the precipitates sizes and L = 41.4 nm is plotted in Figure 5. For small precipitates, τ_c is seen to decrease by 20-30% between 0 and 100 K, and then by only a further 10-20% over the next 500 K. (For voids, the changes are approximately twice as much: see Figure 28 of [44].) For the larger precipitates, i.e. those that partially transform to the FCC-like structure at T = 0 K, the decrease in τ_c is almost constant at approximately 0.2 MPaK^{-1}. These dependences stem from differences in the stress-strain plot as T and D are changed. Figure 6 shows the plots for 2, 4 and 6 nm precipitates for the T values

considered. The shape of the plots is seen is seen to be insensitive to changes in T for small D, but to undergo a transition in form with increasing T for larger D. The maximum transition occurs at about 100 K for D = 4 and 6 nm. No transition occurs for D = 2 nm. This effect is due to the dislocation-induced, partial transformation to the more stable FCC structure reported in the preceding section for T = 0 K.

Confirmation of these trends is to be seen in Figure 7, which shows the $(1\bar{1}0)$ stacking arrangement of Cu atoms near the equator of the 5 nm precipitate after the dislocation has broken away at 1, 300 and 600 K: it should be compared with the low temperature structures for D = 4 and 6 nm in Figure 4. The region of transformed Cu in the 5 nm precipitate reduces with increasing T until it barely exists at 600 K. Mixed climb of the edge dislocation as it breaks for a precipitate is another signature of the transformation process. It was seen in the line shapes for 3 and 4 nm precipitates in [31,32]. The extent of climb is shown by the dislocation core configurations for 5 nm precipitates across the range of temperature in Figure 8. These [111] projections of the core show the bottom of the extra half plane after the dislocation has broken away from the precipitate. There is clearly a stronger tendency for climb with decreasing T, i.e. with increasing volume fraction of transformed Cu. Climb is almost absent at 600 K. Although both climb up and climb down occur, the net effect is climb down, indicating that the transformation is assisted by creation of vacancies within a precipitate. Climb associated with the structural transformation within Cu precipitates contrasts with climb associated with edge dislocation breakaway from voids. In the latter case, the dislocation climbs up by absorbing vacancies from the void and this process occurs for voids of all sizes and at all temperatures in studies by MS and MD, e.g. [31,43.44].

When a precipitate is large enough (D = 6 nm here), dislocation-induced structural transformation of the Cu occurs over the whole temperature range from 0 to 600 K, although the extent of transformation still depends on T. This effect has been quantified by identifying the Cu precipitate atoms whose neighbour coordination is closer to FCC than BCC. (Typically, these atoms have fewer than five BCC neighbours.) The temperature dependence of the fraction of atoms transformed into FCC-like structure in a 6 nm precipitate is plotted in Figure 9. The fraction of transformed atoms increases to its maximum of 0.55 between 0 and 100 K and then declines to 0.1 at 600 K. The increase at low T is believed to reflect the influence on atom mobility of thermal energy. The atomic

configuration of the transformed volume of the 6 nm precipitate at 10, 100 and 600 K is presented in Figures 10(a-c).

Thus, the effects of temperature on dislocation interaction with Cu precipitates in Fe are more complex than those reported elsewhere for voids. They occur because the stability of BCC Cu within a precipitate is dependent on T and D. The free energy difference between the FCC and BCC phases of Cu increases with decreasing T but the surrounding Fe matrix tends to stabilise the BCC phase, and so there is an interplay between precipitate size and temperature in the dislocation-induced transformation process. This can be seen very simply in the critical line shapes for the 2 and 4 nm precipitates at low and high temperature in Figure 11. Both precipitates are sheared at 450 K, as is the 2 nm obstacle at 0 K, but the dislocation-induced transformation within the larger particle at 0 K results in dipole formation and elongation (Orowan) shape characteristic of strong obstacles. Larger precipitates are able to transform at higher temperature (see Figures 9 and 10) and this affects both the critical shape of the dislocation and the critical stress.

5. Discussion

The interatomic potentials of F-S type developed in [2] for the Fe-Cu system have proved to be valuable for many simulation studies of phenomena associated with the creation of radiation damage and changes in mechanical properties in pure Fe and Fe-Cu alloys, as is clear from the number of citations it has received (257 at the time of writing – 29.5.09). In the present paper, we have focused on the obstacle resistance nano-scale Cu precipitates provide to dislocation glide in Fe. The technological relevance of this has been referred to in section 1. It has been seen that modelling based on this interatomic potential predicts a strengthening effect due to a dislocation-induced structural transformation of precipitates that are initially coherent with the surrounding BCC matrix of Fe. This transformation effect was first revealed in MS modelling of a screw dislocation threading Cu precipitates [46]. The size dependence of the Cu transformation mechanism due to screw dislocations has been investigated more recently by MD simulation of screw-precipitate interaction at 10K under constant τ [49]. It was observed that the phase transformation occurred for $D > 1.8$ nm and

that when D exceeds 2.5 nm the dislocation bypass mechanism becomes Orowan looping due to the coherency loss of the precipitates. Values of τ_c were not obtained.

In the present paper, we have extended the data for τ_c reported earlier [31,32] in order to cover a wider range of D and T values and thereby investigate the conditions under which the transformation mechanism is realised. The transformation is due to the difference in the cohesive energy of FCC and BCC copper. However, the thermodynamic driving force for the transformation is small at high temperature and insufficient to provide the energy for loss of coherency for small precipitates. The strengthening effect due to the transformation is therefore realised only for large D and low T in the spectra of size and temperature. The simulations suggest that the yield stress of an under-aged or neutron-irradiated Fe-Cu alloy containing small, coherent precipitates should have a weak T-dependence, whereas the dependence should be stronger in an over-aged or electron-irradiated alloy where the population of coherent precipitates has larger size.

We have referred to strengthening by voids several times in the preceding sections. A final comparison with Cu precipitates illustrates very clearly how the availability of suitable interatomic potentials leads to insight into atomic-scale mechanisms. Figure 12 compares the T-dependence of τ_c for 2, 4 and 6 nm voids and precipitates. The near-coincidence of the curves for D = 6 nm shows that despite the totally different nature of the obstacles, they are both 'strong' and τ_c is determined by the screw dipole arrangement of the dislocation before breakaway occurs. For D = 4 nm, precipitates are weaker obstacles than voids at all T. The difference increases with decreasing size and when D = 2 nm the critical stress for precipitates is only about half that of voids at all temperatures, demonstrating that the energy of the step formed on the Fe-Cu interface and the effect of BCC Cu on the dislocation core energy are not sufficient to stop the dislocation cutting through the precipitate well before the dipole configuration is achieved.

The results described here were obtained for an applied strain rate $\dot{\varepsilon} = 5\text{x}10^6\ \text{s}^{-1}$, but it should be noted that the conclusions drawn are valid across the range of $\dot{\varepsilon}$ that can be used for MD models with millions of atoms. This is shown in Figure 13 by data for τ_c versus $\dot{\varepsilon}$ for 2 and 6 nm precipitates at T = 300 K. The range over several orders of magnitude of $\dot{\varepsilon}$ is the widest that has been reported for simulation of dislocation-obstacle interactions. Figure 13 shows that the influence of obstacle size on τ_c is almost independent of $\dot{\varepsilon}$. In addition, the data indicate that when the strain rate applied in simulations is less than about $5\text{x}10^6\ \text{s}^{-1}$,

the critical stress for these obstacles is independent of $\dot{\varepsilon}$. This limit corresponds to a dislocation velocity in steady state free flight of about 25 ms^{-1} for the model sizes used here.

It is reassuring to point out that direct experimental evidence in support of the predictions from simulation of the influence of *D* and *T* on stability of Cu precipitates during plastic deformation has been obtained by Lozano-Perez et al. [50] by utilising the crystallography of the BCC→9R martensitic transformation. Planes of atoms in twinned 9R precipitates exhibit characteristic 'herring-bone' fringe contrast when viewed along a <111> direction of the Fe matrix in a high-resolution electron microscope (HREM). The angle, α, between fringes in neighbouring twin bands is approximately 129° immediately after the transformation, but relaxes during annealing to 121° to reduce the strain energy [51]. Samples of a Fe-1.3wt%Cu alloy were aged at 550ºC before cooling to room temperature, in order that precipitates larger than about 5 nm would transform to 9R whilst smaller precipitates would retain the BCC structure. One set of samples was plastically deformed by bending at room temperature and both sets were then annealed at 400ºC to allow transformed precipitates to relax. HREM foils were prepared at -60ºC so that any remaining untransformed precipitates should transform to 9R. Angle α was then measured for precipitates in both sets of samples. The results for α versus *D* plotted in Figure 3 of [50] show that precipitates in the undeformed alloy have a relaxation threshold of about 4-5 nm, while all the precipitates in the deformed samples appear to be relaxed. It may be noted that the set of the interatomic potentials used here results in a similar threshold, for the low-temperature transformation was only observed in precipitates with *D* above 4 nm diameter.

Finally, we re-emphasise that a condition for the dislocation-induced transformation mechanism of strengthening discussed here is that the material of the precipitate is metastable when coherent with the surrounding matrix. (Thus, in high-chromium (Cr) ferritic/martensitic steels, Cr-rich α' phase separates from the α phase and forms a fine dispersion of nano-scale obstacles to dislocation motion. Unlike Cu in Fe, Cr is stable in the BCC structure and the strengthening mechanism is different, as demonstrated in the simulations in [52].) Furthermore, the Fe-Cu results show that the energy difference between the metastable and stable structures of the precipitate must not be so large that the transformation occurs without the intervention of a dislocation.

6. Conclusions

(a) The availability of a set of interatomic potentials of Finnis-Sinclair form for the Fe-Cu system has allowed simulation of edge dislocation-Cu precipitate interaction in Fe to be carried out with models containing millions of atoms for a wide range of temperature and applied strain rate.

(b) The simulations reveal that the atomic-scale mechanism that controls the obstacle strength of a precipitate depends on the precipitate size D and ambient temperature T.

(c) The dislocation overcomes small precipitates ($D \leq$ 2-3 nm) at all temperatures by a simple shear mechanism. This results in relatively low critical stress, τ_c, for dislocation breakaway. τ_c for these precipitates has a strong temperature dependence of over the range where edge dislocation glide is thermally-activated ($T <$ approx. 100 K) and a weak dependence above that.

(d) Larger precipitates may transform from the BCC to an FCC-like structure if T is low enough. This effect increases τ_c and results in a critical dislocation shape similar to that of Orowan strengthening, i.e. characterized by zero breaking angle at τ_c, but without creation of an Orowan dislocation loop around the precipitate.

(e) The thermodynamic driving force for the transformation increases with decreasing temperature. However, the surrounding BCC Fe matrix restricts the transformation and this effect lessens with increasing D. Thus, the critical dislocation shape and τ_c exhibit the interplay between T and D, such that even large precipitates are weak obstacles at high T.

(f) The dislocation-induced transformation effects are clearly seen in visualisations of the stacking sequence and FCC-like neighbour coordination of Cu atoms after dislocation breakaway.

(g) The effects found by simulation are consistent with the results of HREM experiments on deformed Fe-Cu alloy reported in [50].

(h) The results presented for the dislocation-precipitate interaction mechanism and its dependence on T and D imply that the temperature dependence of the yield stress of under-aged or neutron-irradiated Fe-Cu alloys should be different from that of over-aged or electron-irradiated alloys.

Acknowledgements

This work was supported by the Division of Materials Sciences and Engineering and the Office of Fusion Energy Sciences, U.S. Department of Energy, under contract DE-AC05-00OR22725 with UT-Battelle, LLC; and grant GR/R68870/01 from the UK Engineering and Physical Sciences Research Council.

References

1. M.W. Finnis and J.E. Sinclair, Phil. Mag. A 53 (1984) p.45.
2. G.J. Ackland, D.J. Bacon, A.F. Calder and T. Harry, Phil. Mag. A 75 (1997) p.713.
3. R. Monzen, M.L. Jenkins, A.P. Sutton, Philos. Mag. A 80 (2000) p.711.
4. J.T. Buswell, C.A. English, M.G. Hetherington, W.J. Phythian, G.D.W. Smith, G.M. Worral, Effects of Radiation on Materials: 14th Int. Sympos. ASTM STP 1046, vol. II, ASTM, Philadelphia, PA, 1990, p.127.
5. R.G. Carter, N. Soneda, K. Dohi, J.M. Hyde, C.A. English, W.L. Server, J. Nucl. Mater. 298 (2001) p.211.
6. R. Chaouadi, R. Gerard, J. Nucl. Mater. 345 (2005) p.65.
7. G.J. Ackland, G. Tichy, V. Vitek and M.V. Finnis, Phil. Mag. A 56 (1987) p.735.
8. A.F. Calder and D.J. Bacon, in *Microstructure Evolution During Irradiation* (eds. I.M. Robertson, G.S. Was, L.W. Hobbs and T. Diaz de la Rubia), MRS Sympos. Proc. vol. 439 (1997) p. 521.
9. D.J. Bacon, Yu.N. Osetsky and R.E. Stoller, J. Nucl. Mater. 323 (2003) p.152.
10. C.S. Becquart, C. Domain, A. Legris, J.C. Van Duysen, J. Nucl. Mater. 280 (2000) p.73.
11. A. Souidi, C.S. Becquart, C. Domain, D. Terentyev, L. Malerba, A.F. Calder, D.J. Bacon, R.E. Stoller, Yu.N. Osetsky and M. Hou, J. Nucl. Mater. 355 (2006) p.89.
12. A.F. Calder, D.J. Bacon, A.V. Barashev and Yu.N. Osetsky, Phil. Mag. Lett. 88 (2008) p.43.
13. Yu.N. Osetsky, M. Victoria, A. Serra, S.I. Golubov and V. Priego, J. Nucl. Mater. 251 (1997) p.34.
14. A.V. Barashev, Yu.N. Osetsky and D.J. Bacon, Philos. Mag. 80 (2000) p.2709.
15. Yu.N. Osetsky, A. Serra and V. Priego, J. Nucl. Mater. 276 (2000) p.202.
16. M.A. Puigvi, Yu.N. Osetsky and A. Serra, Philos. Mag. 83 (2003) p.857.
17. Yu.N. Osetsky, D.J. Bacon and A. Serra, Philos. Mag. 83 (2003) p.61.
18. F. Gao, H. Heinisch, R.J. Kurtz, Yu.N. Osetsky and R.G. Hoagland, Philos. Mag. 85 (2005) p.619.
19. J. Marian, B.D. Wirth, J.M. Perlado, G.R. Odette and T. Diaz de la Rubia, Phys. Rev. B 64 (2001) 094303.

20. J. Marian, B.D. Wirth, A. Caro, B. Sadigh, G.R. Odette, J.M. Perlado and T. Diaz de la Rubia, Phys. Rev. B 65 (2002) 144102.
21. J. Marian, B.D. Wirth, G.R. Odette and J.M. Perlado, Comput. Mater. Sci. 31 (2004) p.347.
22. Yu.N. Osetsky, A. Serra, M. Victoria, S.I. Golubov and V. Priego, Phil. Mag. 79 (1999) p.2259; *ibid:* p.2285.
23. Yu.N. Osetsky, D.J. Bacon and V. Mohles, Phil. Mag. 83 (2003) p.3623.
24. Yu.N. Osetsky and D.J. Bacon, J. Nucl. Mater. 323 (2003) p.268.
25. Yu.N. Osetsky and D.J. Bacon, Mater. Sci. Eng. A 400-401 (2005) p.374.
26. D. Terentyev, D.J. Bacon and Yu.N. Osetsky, J. Phys. Condens. Matter 20 (2008) p.445007.
27. D.J. Bacon, Yu.N. Osetsky and Z. Rong, Phil. Mag. 86 (2006) p.3921.
28. D. Terentyev, P. Grammatikopoulos, D.J. Bacon, Yu. N. Osetsky, Acta Mater. 56 (2008) p.5034.
29. Yu.N. Osetsky, D. Rodney and D.J. Bacon, Philos. Mag. 86 (2006) p.2295.
30. Yu.N. Osetsky, Y. Matsukawa, and R.E. Stoller, J. Nucl. Mater. 329 (2004) p. 1228.
31. Yu.N. Osetsky, D.J. Bacon and V. Mohles, Phil. Mag. 83 (2003) p.3623.
32. D.J. Bacon and Y.N. Osetsky, J. Nucl. Mater. 329-333 (2004) p.1233.
33. J.J. Blackstock and G. J. Ackland, Philos. Mag. A, 81 (2001) p.212.
34. A. Machov, Comput. Mater. Sci. 24 (2002) p.535.
35. A.C. Arokiam, A.V. Barashev, D.J. Bacon and Yu.N. Osetsky, Philos. Mag. Lett. 85 (2005) p.491.
36. D. Kulikov, L. Malerba and M. Hou, Philos. Mag. 86 (2006) p.141.
37. M. Ludwig, D. Farkas, D. Pedraza and S. Schmauder, Modelling Simul. Mater. Sci. Eng. 6 (1998) p.19.
38. G.J. Ackland, M.I. Mendelev, D.J. Srolovitz, S. Han et al., J. Phys. Condens. Matter 16 (2004) S2629.
39. Yu.N. Osetsky and D.J. Bacon, Modelling Simul. Mater. Sci. Eng. 11 (2003) p.427.
40. D.J. Bacon, U.F. Kocks and R.O. Scattergood, Phil. Mag. 28 (1973) p.1241.
41. R.O. Scattergood and D.J. Bacon, Acta Metall. 30 (1982) p.1665.
42. D.J. Bacon, in *Fundamentals of Deformation and Fracture* (eds B.A. Bilby, K.J. Miller and J.R. Willis), Cambridge University Press (1985) p.401.

43. D.J. Bacon and Yu.N. Osetsky, Math. Mech. Solids 14 (2009) p.270.
44. D.J. Bacon, Yu.N. Osetsky and D. Rodney, in *Dislocations in Solids* (eds. J.P. Hirth and L. Kubin), Elsevier, Amsterdam (2009) chap. 88, vol.15, in the press.
45. D. Hull and D.J. Bacon, *Introduction to Dislocations*, Butterworth-Heinemann, Oxford, 2001.
46. T. Harry and D.J. Bacon, Acta Mater. 50 (2002a) p.195; (2002b) p.209.
47. K.C. Russell and L.M. Brown, Acta Metall. 20 (1972) p.969.
48. Yu.N. Osetsky and D.J. Bacon, J. Nucl. Mater. 323 (2003) p.268.
49. J.H. Shim, Y.W. Cho, S.C. Kwon, W.W. Kim, B.D. Wirth, Appl. Phys. Lett. 90 (2007) p.021906.
50. S. Lozano-Perez, M.L. Jenkins, J.M. Titchmarsh, Philos. Mag. Lett. 86 (2006) p.367.
51. R. Monzen, M.L. Jenkins and A.P. Sutton, Philos. Mag. A 80 (2000) p.711.
52. D.A. Terentyev, G. Bonny, L. Malerba, Acta Mater. 56 (2008) p.3229.

Figure captions

Fig. 1. Stress-strain curves obtained for interaction between an edge dislocation and Cu precipitates with spacing L = 41.4 nm and diameter D as indicated in Fe at 0 K.

Fig. 2. Critical line shape in the $(1\bar{1}0)$ slip plane for a dislocation passing a row of either spherical voids or Cu precipitates with L = 62 nm and D in the range 0.9-5 nm size in Fe at 0 K. Black line: shape for voids; grey line: shape for precipitates. The labels for each pair of shapes indicate: τ_c for void, D and τ_c for precipitate, in descending order.

Fig. 3. Critical stress τ_c (units Gb/L) versus the harmonic mean of D and L (unit b) for voids (circles) and Cu precipitates (triangles) in Fe at 0 K for all the values of D (0.9-6 nm) and L (41.4-83.6 nm) considered. Lines found in [40.41] to be best fits to τ_c values obtained in continuum modelling for voids and impenetrable Orowan particles are also shown.

Fig. 4. Position of Cu atoms in four consecutive $(1\bar{1}0)$ planes through the centre of a precipitate in Fe after dislocation breakaway. (a) 4 nm precipitate at 0 K; (b) 6 nm precipitate at 10 K.

Fig. 5. Plot of τ_c versus T for Cu precipitates in Fe. D is as indicated, L = 41.4 nm and $\dot{\varepsilon}$ = $5\text{x}10^6\text{s}^{-1}$.

Fig. 6. Stress-strain curves for interaction between an edge dislocation and Cu precipitates with spacing L = 41.4 nm in Fe strained at $5\text{x}10^6$ s^{-1}. (a) D = 2 nm and T = 1 to 450 K; (b) D = 4 nm and T = 1 to 450 K; (c) D = 6 nm and T = 1 to 600 K.

Fig. 7. Position of Cu atoms in four consecutive $(1\bar{1}0)$ planes through the centre of a 5 nm precipitate in Fe after dislocation breakaway at (a) 1 K, (b) 300 K and (c) 600 K.

Fig. 8. Core of the edge dislocation line in [111] projection after breakaway from a 5 nm Cu precipitate in Fe at the temperatures indicated. Climb up indicates absorption of vacancies from the precipitate whereas climb down is due to creation of vacancies in the precipitate.

Fig.9. Temperature-dependence of the fraction of the atoms transformed into FCC-like structure in 6 nm precipitate after dislocation breakaway.

Fig.10. Configuration of the atoms transformed into FCC-like structure inside a 6 nm precipitate after dislocation breakaway at (a) 10 K, (b) 100 K (maximum transformed fraction) and (c) 600 K.

Fig. 11. Critical line shape in the $(1\bar{1}0)$ plane for a dislocation passing a row of (a) 2 nm and (b) 4 nm Cu precipitates with spacing 41.4 nm in Fe at the temperature indicated.

Fig. 12. Plots of τ_c versus T for Cu precipitates and voids in Fe for D = 2, 4 and 6 nm, as indicated. L = 41.4 nm and $\dot{\varepsilon} = 5\text{x}10^{6}\text{s}^{-1}$.

Fig. 13. Variation of τ_c with applied strain rate for 2 and 6 nm Cu precipitates (triangles) and voids (circles) in Fe at 300 K. The dislocation velocity, V_d, in steady state flight depends on the model size through the Orowan relation between $\dot{\varepsilon}$, V_d and dislocation density [45]. For the lowest value $\dot{\varepsilon} = 10^{5}\text{s}^{-1}$ here, V_d = 0.5 ms^{-1}, as indicated.

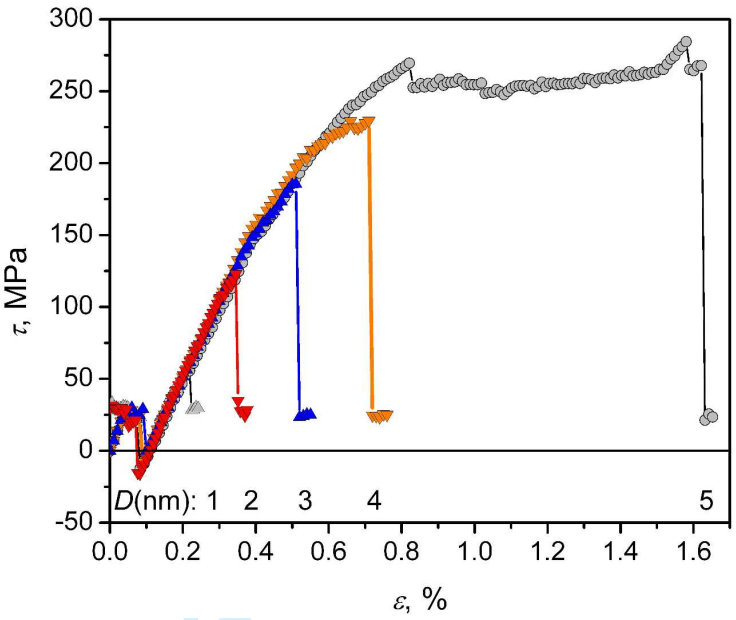

Fig. 1. Stress-strain curves obtained for interaction between an edge dislocation and Cu precipitates with spacing $L = 41.4$ nm and diameter D as indicated in Fe at 0 K.

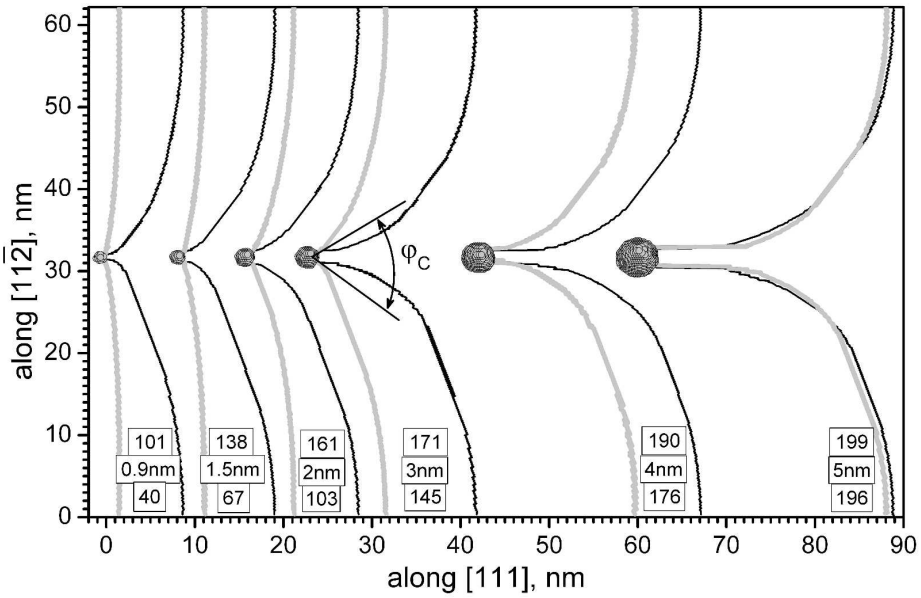

Fig. 2. Critical line shape in the $(1\,\bar{1}0)$ slip plane for a dislocation passing a row of either spherical voids or Cu precipitates with $L = 62$ nm and D in the range 0.9-5 nm size in Fe at 0 K. Black line: shape for voids; grey line: shape for precipitates. The labels for each pair of shapes indicate: τ_c for void, D and τ_c for precipitate, in descending order.

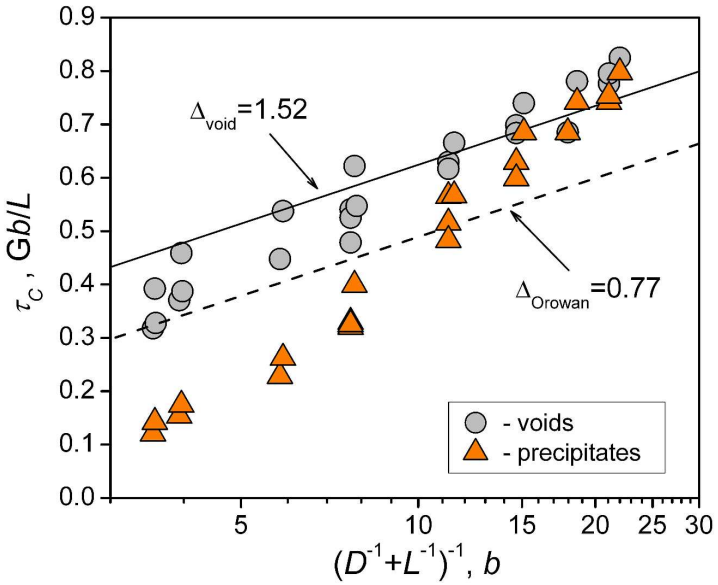

Fig. 3. Critical stress τ_c (units Gb/L) versus the harmonic mean of D and L (unit b) for voids (circles) and Cu precipitates (triangles) in Fe at 0 K for all the values of D (0.9-6 nm) and L (41.4-83.6 nm) considered. Lines found in [40.41] to be best fits to τ_c values obtained in continuum modelling for voids and impenetrable Orowan particles are also shown.

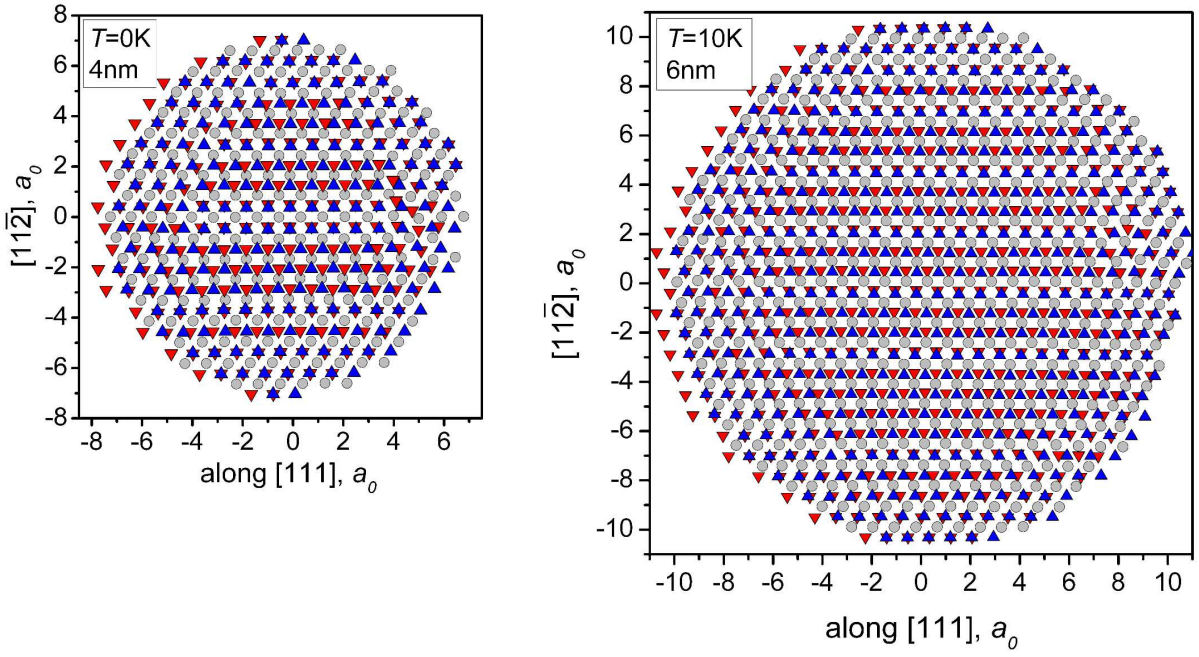

Fig. 4. Position of Cu atoms in four consecutive $(1\bar{1}0)$ planes through the centre of a precipitate in Fe after dislocation breakaway. (a) 4 nm precipitate at 0 K; (b) 6 nm precipitate at 10 K.

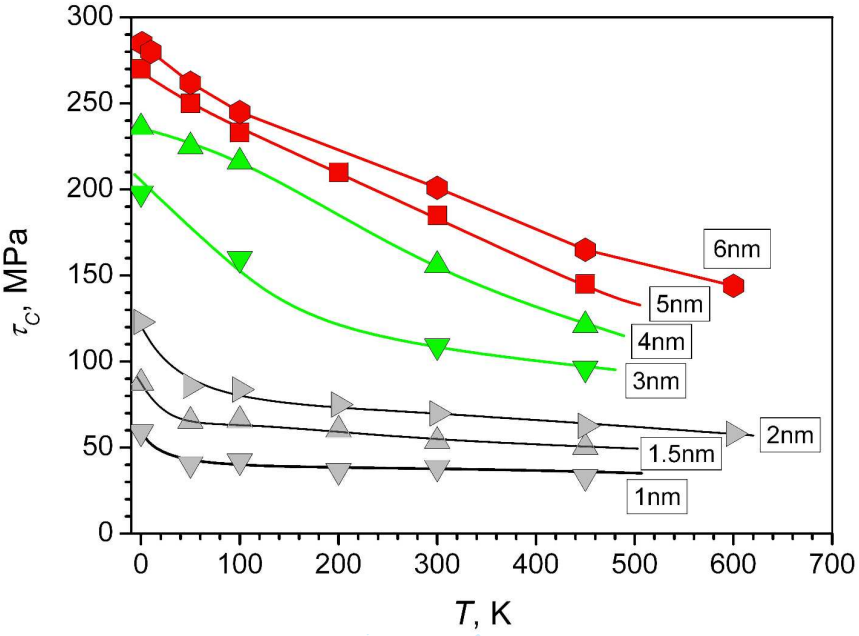

Fig. 5. Plot of τ_c versus T for Cu precipitates in Fe. D is as indicated, $L = 41.4$ nm and $\dot{\varepsilon} = 5\text{x}10^{6}\text{s}^{-1}$.

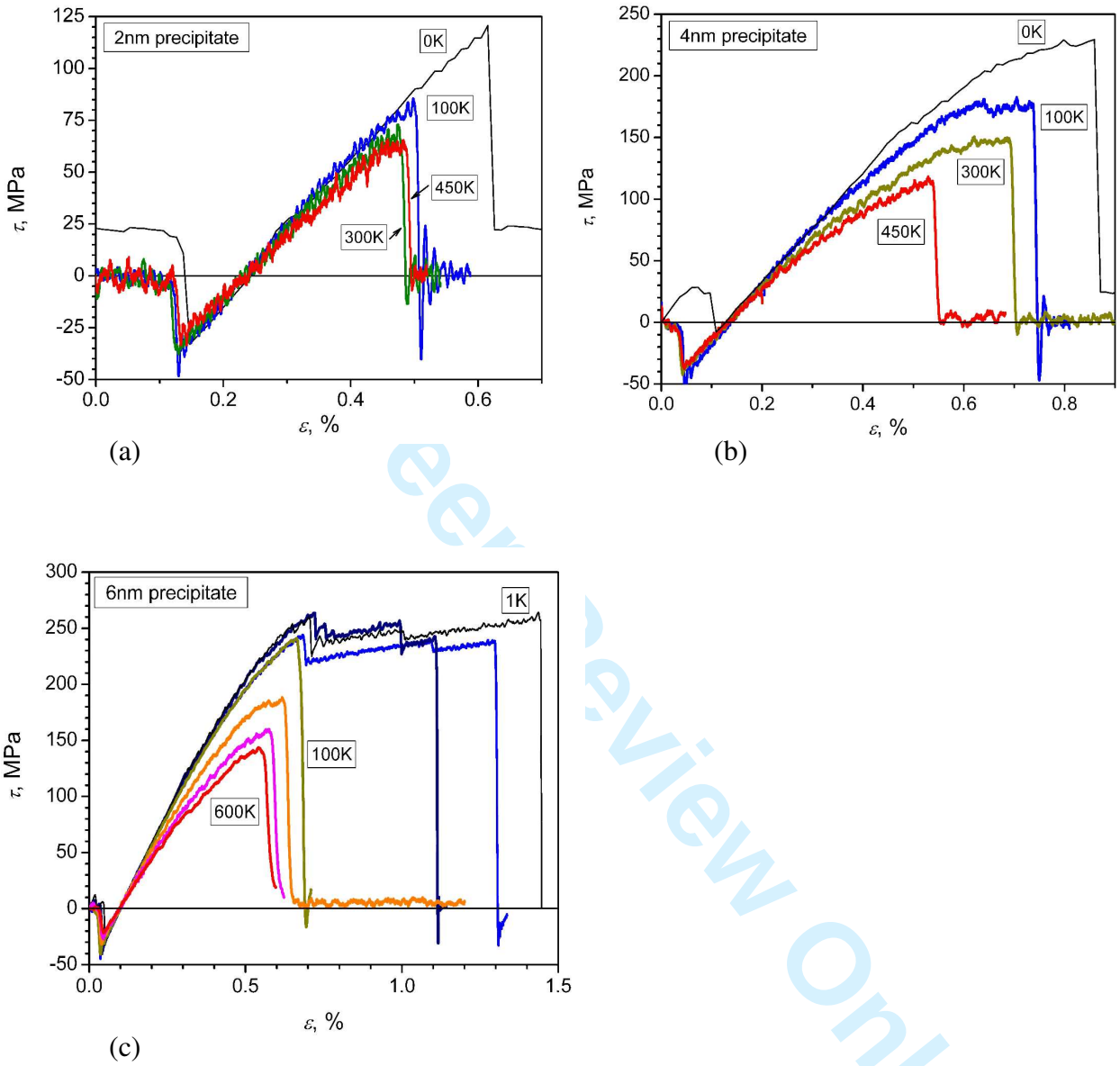

Fig. 6. Stress-strain curves for interaction between an edge dislocation and Cu precipitates with spacing $L = 41.4$ nm in Fe strained at 5×10^6 s^{-1}. (a) $D = 2$ nm and $T = 1$ to 450 K; (b) $D = 4$ nm and $T = 1$ to 450 K; (c) $D = 6$ nm and $T = 1$ to 600 K.

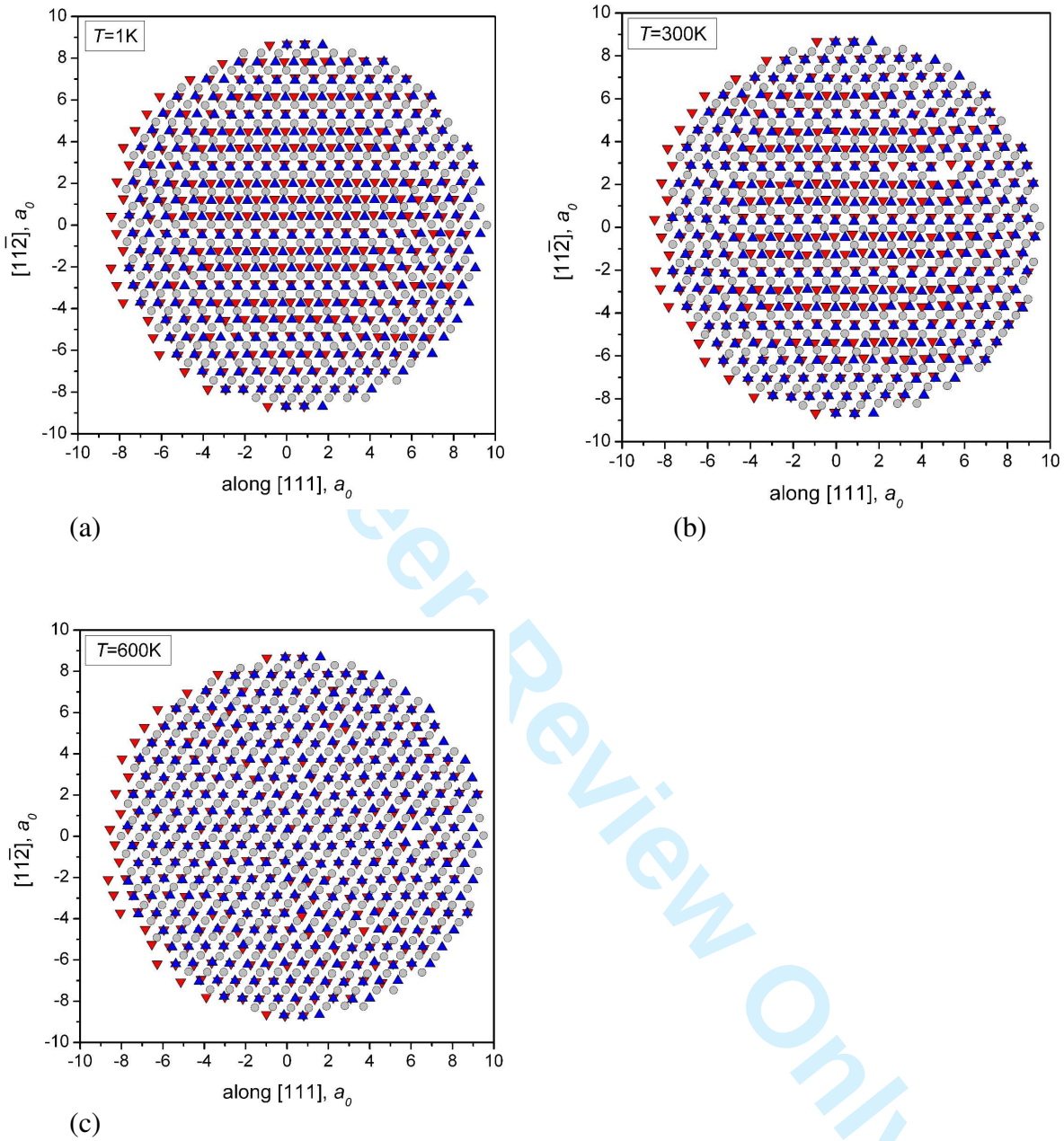

Fig. 7. Position of Cu atoms in four consecutive $(1\,\bar{1}0)$ planes through the centre of a 5 nm precipitate in Fe after dislocation breakaway at (a) 1 K, (b) 300 K and (c) 600 K.

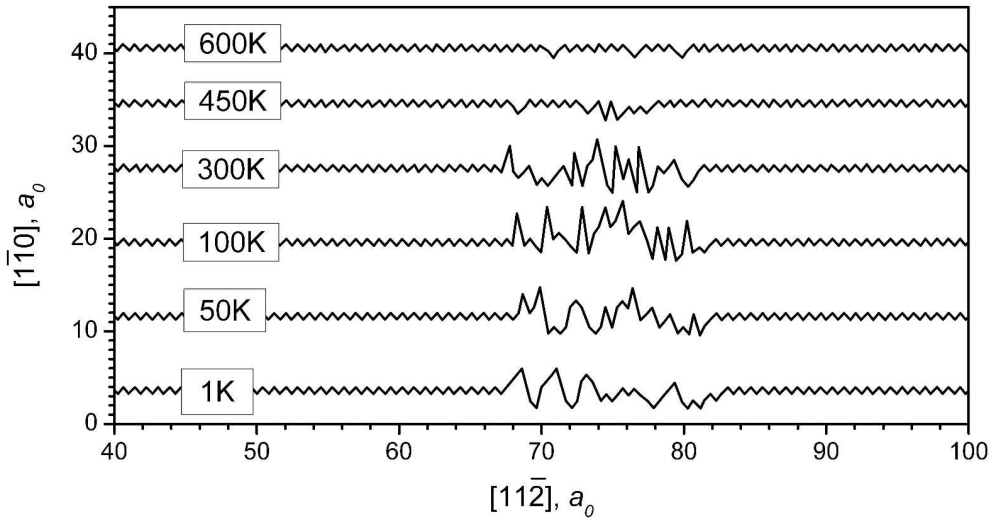

Fig. 8. Core of the edge dislocation line in [111] projection after breakaway from a 5 nm Cu precipitate in Fe at the temperatures indicated. Climb up indicates absorption of vacancies from the precipitate whereas climb down is due to creation of vacancies in the precipitate.

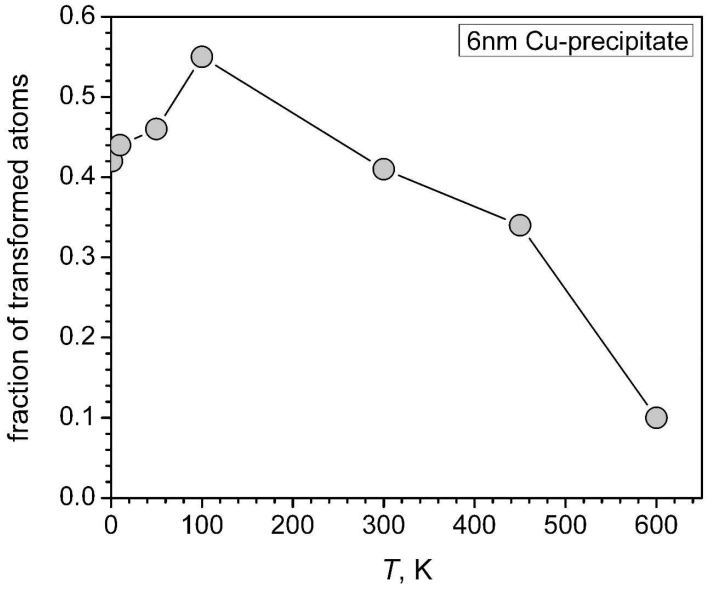

Fig. 9. Temperature-dependence of the fraction of the atoms transformed into FCC-like structure in 6 nm precipitate after dislocation breakaway.

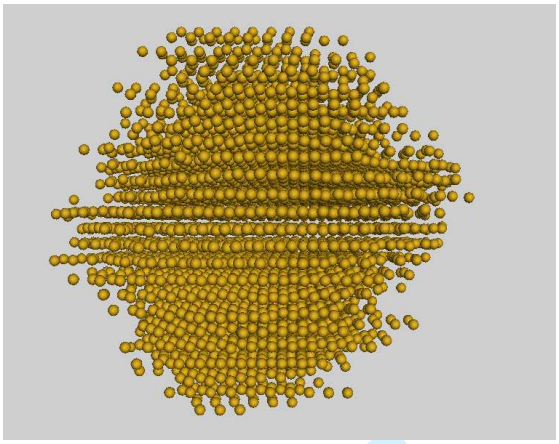

(a)

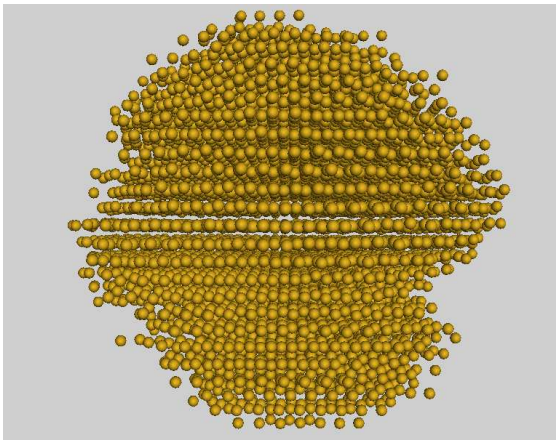

(b)

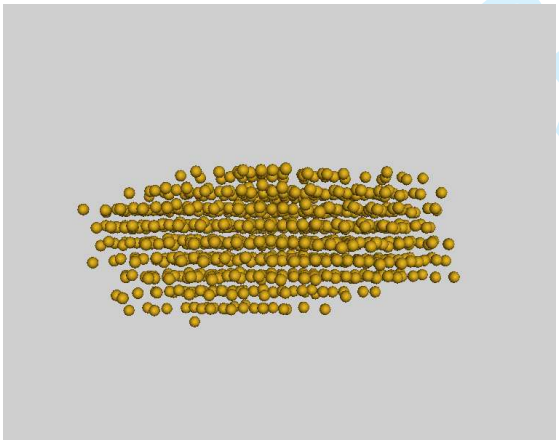

(c)

Fig. 10. Configuration of the atoms transformed into FCC-like structure inside a 6 nm precipitate after dislocation breakaway at (a) 10 K, (b) 100 K (maximum transformed fraction) and (c) 600 K.

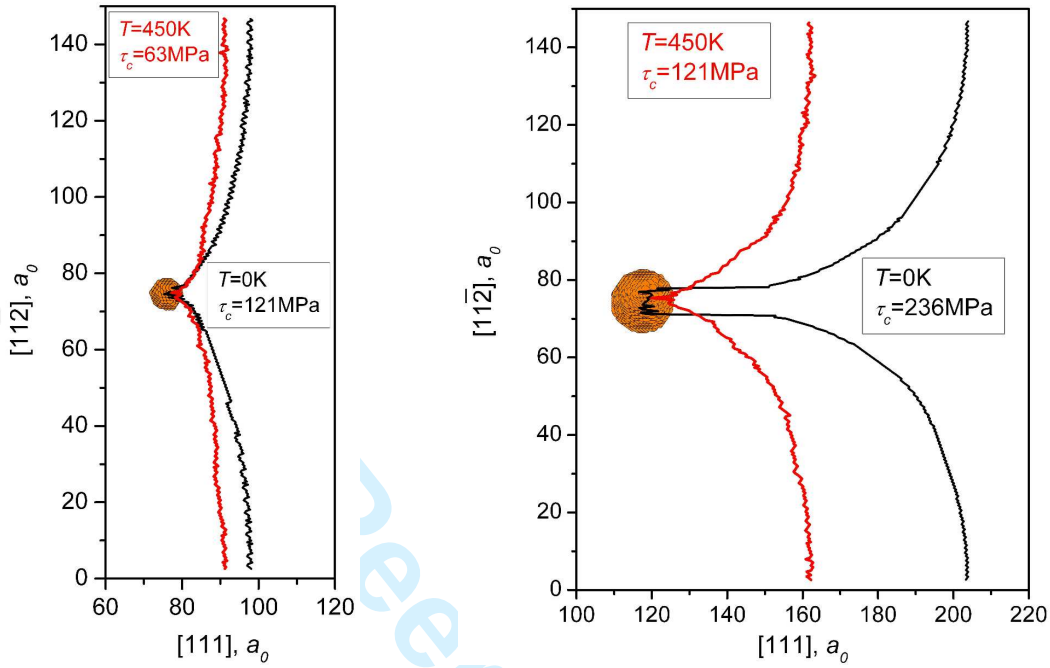

(a) (b)

Fig. 11. Critical line shape in the $(1\bar{1}0)$ plane for a dislocation passing a row of (a) 2 nm and (b) 4 nm Cu precipitates with spacing 41.4 nm in Fe at the temperature indicated.

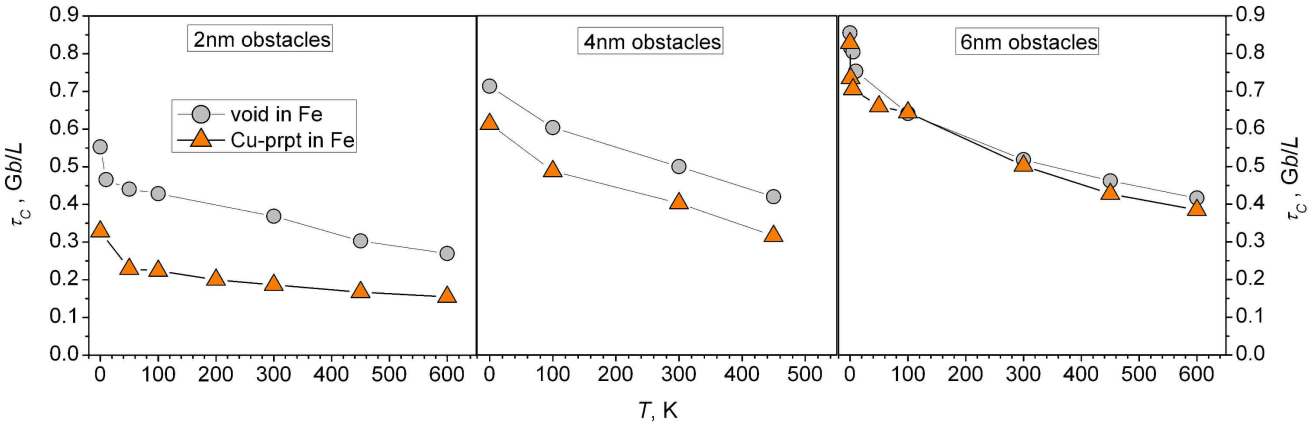

Fig. 12. Plots of τ_c versus T for Cu precipitates and voids in Fe for D = 2, 4 and 6 nm, as indicated. L = 41.4 nm and $\dot{\varepsilon} = 5\text{x}10^{6}\text{s}^{-1}$.

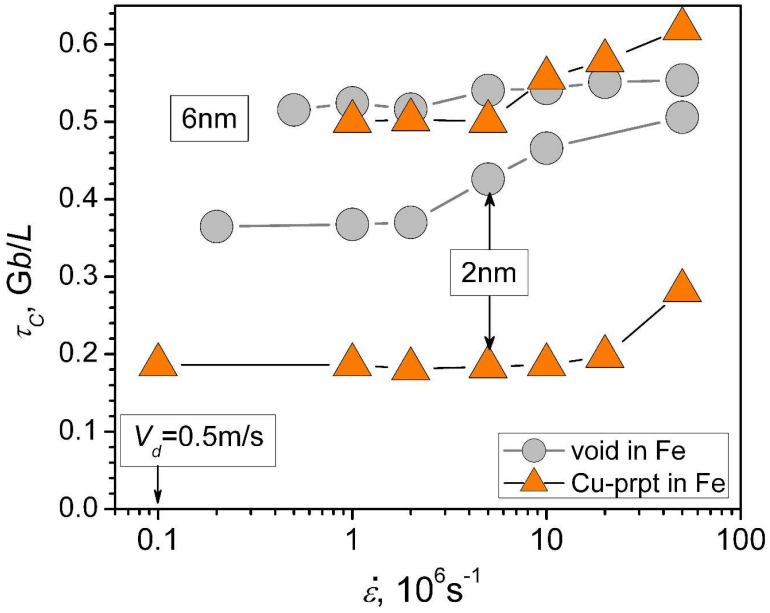

Fig. 13. Variation of τ_c with applied strain rate for 2 and 6 nm Cu precipitates (triangles) and voids (circles) in Fe at 300 K. The dislocation velocity, V_d, in steady state flight depends on the model size through the Orowan relation between $\dot{\varepsilon}$, V_d and dislocation density [45]. For the lowest value $\dot{\varepsilon} = 10^5 s^{-1}$ here, $V_d = 0.5$ ms^{-1}, as indicated.